Published in final edited form as:

Nat Genet. 2011 May 8; 43: 547–553. doi:10.1038/ng.832.

Complex Interactions Between Genes Controlling Trafficking in Primary Cilia

Polloneal Jymmiel R. Ocbina[1,2,6], **Jonathan T. Eggenschwiler**[3], **Ivan P. Moskowitz**[4,5], and **Kathryn V. Anderson**[1,7]

[1] Developmental Biology Program Sloan-Kettering Institute 1275 York Avenue New York, NY 10065

[2] Neuroscience Program, Weill Graduate School of Medical Sciences, Cornell University 445 East 69th Street New York, NY 10065

[3] Department of Molecular Biology, Princeton University, Princeton, NJ 08544

[4] Department of Pediatrics, The University of Chicago, Chicago, IL, 60637, USA

[5] Department of Pathology, The University of Chicago, Chicago, IL, 60637, USA

Abstract

Cilia-associated human genetic disorders are striking in the diversity of their abnormalities and their complex inheritance. Inactivation of the retrograde ciliary motor by mutations in *DYNC2H1* cause skeletal dysplasias that have strongly variable expressivity. Here we define unexpected genetic relationships between *Dync2h1* and other genes required for ciliary trafficking. Mutations in mouse *Dync2h1* disrupt cilia structure, block Sonic hedgehog (Shh) signaling and cause midgestation lethality. Heterozygosity for *Ift172*, a gene required for anterograde ciliary trafficking, suppresses the cilia phenotypes, Shh signaling defects and early lethality of *Dync2h1* homozygotes. *Ift122*, like *Dync2h1*, is required for retrograde ciliary trafficking, but reduction of the *Ift122* gene dosage also suppresses the *Dync2h1* phenotype. These genetic interactions illustrate the cell biology underlying ciliopathies and argue that mutations in IFT genes cause their phenotypes because of their roles in cilia architecture rather than direct roles in signaling.

Introduction

Human ciliopathies arise from defects in the primary cilium and can lead to obesity, retinal degeneration and cystic kidney disease, and are also associated with a wide array of morphological abnormalities. Although most of the characterized ciliopathies are single gene recessive disorders, there is evidence that mutations in more than one cilia-associated gene can have additive or synergistic effects in disease [1-5]. It has been estimated that there

[7] Corresponding author: k-anderson@sloankettering.edu.
[6]Current address: Department of Genetics, Yale University School of Medicine, New Haven, CT 06510

Author Contributions: P.J.O. and K.V.A. conceived the experiments and wrote the manuscript; P.J.O performed experiments; J.T.E. helped write the manuscript and provided reagents; I.M. provided reagents.

are more than 100 cilia-associated human diseases [6] and that hundreds of genes are required for the construction of cilia and the centrioles that template cilia [7,8], making ciliopathies a model for the complex genetic interactions seen in human genetic disease.

Mutations in human *DYNC2H1*, which encodes the heavy chain of the cytoplasmic dynein-2 motor required for trafficking cargo from the tip to the base of the cilium, have been associated with short rib-polydactyly syndrome (SRP) type III and Jeune asphyxiating thoracic dystrophy (JATD) [9,10], two related skeletal dysplasias characterized by shortened long bones, a narrow rib cage and polydactyly, and other features of ciliopathies. Assembly of cilia depends on the process of intraflagellar transport (IFT) [11]. IFT particles, composed of IFT-A and IFT-B protein complexes, are transported to the tip of the cilium (anterograde transport) by the heterotrimeric kinesin-2, and transport of products back to the base of the cilium (retrograde transport) is powered by cytoplasmic dynein-2. Chondrocyte cilia from individuals with *DYNC2H1* mutations are shortened with bulbous distal ends, similar to the phenotypes of IFT-dynein mutant cilia in other species [10]. The human syndromes show a range of severity, from lethality during gestation to adult survival in affected individuals, with no apparent relationship between the nature of the mutation and the severity of the disease [9]. The presence of both SRP type III and the less severe JATD within the same family also suggests that the human phenotypes can be modified by other genetic or environmental factors [12].

Many of the morphological abnormalities seen in human ciliopathies are likely to be caused by disruption of the Hedgehog (Hh) signaling pathway [13,14]. Genetic analysis in the mouse and zebrafish has shown that primary cilia are essential for Hh signal transduction in vertebrate embryos [13]. Mutations in all of the IFT genes that have been studied disrupt Hh signaling. For example, mouse mutants that lack IFT-B complex proteins lack cilia and fail to respond to Hh signals; these mutants can neither activate Hh target genes nor produce the Gli repressors that keep target genes off in the absence of ligand [15,16].

The proteins that mediate Hedgehog signal transduction are enriched in wild-type primary cilia. Patched1 (Ptch1), the Hh receptor, is present in cilia in the absence of ligand, but moves out in response to Hh ligand [17]. The transmembrane protein Smoothened (Smo), which acts downstream of Ptch1 moves into cilia in response to Shh, and cilia localization of Smo is required to activate downstream signaling [17,18]. The Gli2 and Gli3 transcription factors that implement Hh signals are enriched at the tips of cilia [19], and the level of Gli2 and Gli3 at cilia tips increases in response to ligand [20,21]. It is, however, unclear how or whether IFT directly regulates trafficking of specific components of the Hh signal transduction pathway.

Mouse *Dync2h1* mutants show a loss of Shh-dependent signaling in the neural tube and die at midgestation (~e10.5) [15,22]. Here we define the genetic relationships between *Dync2h1* and other genes required for ciliogenesis. Unexpectedly, we find that both the cilia morphology and Shh phenotypes of *Dync2h1* homozygotes are strongly suppressed when the level of either the IFT-A or IFT-B proteins is reduced. The results indicate that the balance of anterograde and retrograde IFT controls ciliary architecture, which in turn controls Shh signaling and the developmental processes that are disrupted in ciliopathies.

Results

Dync2h1 mutant alleles disrupt Sonic hedgehog signal transduction and cilia structure

Shh-dependent neural patterning is blocked in each of the *Dync2h1* mutants that have been studied, including apparent null alleles (Fig. 1a, Supplementary Fig. 1) [15,22,23]. The ventral neural cell types specified by the highest level of Shh signaling, the floor plate and V3 interneuron progenitors, are never specified in any of the mouse *Dync2h1* mutants (Fig. 1a, Supplementary Fig. 1a, b) [15,22,23]. Motor neurons, which are specified by intermediate levels of Shh, are greatly reduced in number in the rostral neural tube (Supplementary Fig. 2), but do develop caudally (Fig. 1a, Supplementary Fig. 1b). Double mutant analysis showed that *Dync2h1* is required for the activity of the Hh pathway at the heart of the signal transduction pathway, downstream of Ptch1 and upstream of the Gli transcription factors (Supplementary Fig. 2), like other IFT genes [16,24].

Scanning electron microscopy (SEM) analysis of primary cilia in the neural tube showed that, while there were some differences in cilia morphology between different *Dync2h1* alleles, all mutant cilia appeared swollen (Fig. 1b, Supplementary Fig. 1c). *Dync2h1*$^{lln/lln}$ cilia were the least affected of the *Dync2h1* mutants; these cilia were as long as in wild type, but were twice as wide (Supplementary Table 1). We found that twice as much IFT88, a component of the IFT-B complex, accumulated in *Dync2h1*$^{lln/lln}$ ciliary axonemes (Fig. 1c, Supplementary Table 2), similar to the accumulation of IFT particles in *Chlamydomonas* dynein-2 mutant flagella [25-27].

In contrast to the restricted, Shh-dependent localization of Shh pathway proteins in wild-type cilia, we observed previously that Smo accumulates in cilia of *Dync2h1*$^{ttn/ttn}$ mutant mouse embryo fibroblasts (MEFs) [23] and over-expressed Gli2 accumulates to high levels in *Dync2h1* RNAi-treated cells [28]. We examined the localization of Hh pathway proteins in *Dync2h1*$^{lln/lln}$ MEFs (Fig. 2), and found that high levels of Smo, Gli2 and Ptch1 accumulated along the entire length of *Dync2h1*$^{lln/lln}$ ciliary axoneme in the absence or presence of Shh (Fig. 2a, c, e, Supplementary Table 3). We also examined the cilia on the neural progenitors that project into the lumen of the developing neural tube and found that Smo, Gli2 and Ptch1 accumulated to high levels in the cilia at both ventral positions, near the source of Shh, and dorsally, far from any Shh (Fig. 2b, d, f, Supplementary Fig. 3). Thus, even in the absence of ligand, Smo, Gli2 and Ptch1 traffic into cilia and accumulate there in the absence of the IFT-dynein retrograde motor.

Decreased activity of IFT-B suppresses the defects in Shh signaling, cilia morphology and Hh pathway protein localization of *Dync2h1* homozygotes

Because Hh pathway proteins accumulate in primary cilia in the absence of the retrograde motor, we tested whether reduction of anterograde trafficking within the cilium would affect the *Dync2h1*$^{lln/lln}$ phenotypes. The IFT-B protein complex is required for anterograde trafficking, and null mutations in IFT-B genes block ciliogenesis [16]. As expected, mutants that were homozygous for both *Dync2h1*^{lln} and a null allele of an IFT-B gene, *Ift172*^{wim}, were indistinguishable from *Ift172*^{wim} homozygotes: they lacked cilia and embryos failed to specify all ventral neural cell types (Supplementary Fig. 4a). We then examined the

Dync2h1^{lln} phenotype when combined with *avc1*, a partial loss-of-function allele of *Ift172* [29,30]. While neural patterning in *Ift172*$^{avc1/avc1}$ mutants was nearly wild type (Supplementary Fig. 4a), *Dync2h1*$^{lln/lln}$ *Ift172*$^{avc1/avc1}$ double mutants lacked floor plate and V3 progenitors, as in *Dync2h1*$^{lln/lln}$ but did specify motor neurons rostrally as well as caudally, suggesting that *Ift172*$^{avc1/avc1}$ partially rescued the *Dync2h1*$^{lln/lln}$ phenotype (Supplementary Fig. 4).

A more dramatic rescue of the *Dync2h1* phenotype was observed in *Dync2h1*$^{lln/lln}$ *Ift172*^{avc1}/+ compound mutants. All Shh-dependent ventral neural cell types were specified in the compound mutants, including the floor plate, which expressed FoxA2, and Nkx2.2-expressing V3 progenitors (Fig. 3a). A similar, but less complete, rescue of Shh-dependent neural patterning was seen in *Dync2h1*^{lln} homozygotes that were heterozygous for null alleles of *Ift172* or of another IFT-B complex gene, *Ift88* (Supplementary Fig. 5), although *Ift172*^{wim}/+, *Ift88*^{null}/+ and *Ift172*^{avc1}/+ animals have no detectable phenotype. While all *Dync2h1*$^{lln/lln}$ mutants die by E13.5 [15], ~30% of *Dync2h1*$^{lln/lln}$ *Ift172*^{avc1}/+ embryos survived to at least E16.5 (Fig. 3b). IFT mutants that survive long enough to make digits are polydactylous due to the failure to make Gli3 repressor [15,22,24,31-33]. At E16.5, some *Dync2h1*$^{lln/lln}$ *Ift172*^{avc1}/+ mutants (n=2/5) did not exhibit polydactyly in either forelimbs or hindlimbs (Fig. 3c, Supplementary Fig. 6). Thus a modest reduction of IFT-B proteins rescued the early lethality and polydactyly caused by the absence of IFT-dynein function.

In parallel with this rescue of Shh signaling, the morphology of primary cilia in the neural tube of *Dync2h1*$^{lln/lln}$ *Ift172*^{avc1}/+ was also rescued, as assayed by SEM (Fig 3d). The IFT-B complex protein IFT88 did not accumulate in the compound mutant cilia (Fig. 3e). In contrast to the accumulation of Smo in the absence of ligand in *Dync2h1*$^{lln/lln}$ MEFs (Fig. 2a), Smo was detected in cilia of *Dync2h1*$^{lln/lln}$ *Ift172*^{avc1}/+ compound mutant cells only after stimulation with Shh (Fig. 3f), as in wild type. Gli2 was observed only at cilia tips in *Dync2h1*$^{lln/lln}$ *Ift172*^{avc1}/+ mutants (Fig. 3g), as in wild type and at more normal levels (Supplementary Table 3). Thus, reduction of the level of IFT-B, and presumably a decreased rate of anterograde trafficking, bypassed the requirement for the IFT-dynein for both cilia structure and Shh signaling.

Hh pathway activation in the absence of both the IFT-A protein IFT122 and Dync2h1

Retrograde trafficking depends on both IFT-dynein and the IFT-A complex [25,26,34,35]. Mouse mutants that lack the IFT-A complex genes *Ift122* and *Ttc21b* (the mouse orthologue of *Chlamydomonas reinhardtii* IFT-A complex gene *Ift139*) have short bulbous cilia [24,36] and depletion of TTC21B causes slower retrograde IFT without affecting anterograde IFT [24], indicating that the function of IFT-A proteins in retrograde trafficking is conserved in mammals. However, in contrast to *Dync2h1* mutants where the block in retrograde transport prevents the response to Shh, *Ift139* and *Ift122* mutants show ligand-independent ectopic activation of the Shh pathway [24,32].

One hypothesis to explain the block of Hh signaling in *Dync2h1* mutant embryos is that Gli proteins are trapped in the cilium by the defect in retrograde trafficking and therefore cannot activate target genes in the nucleus. If this were correct, then *Dync2h1 IFT-A* double mutant embryos should have a strong defect in retrograde trafficking and would be expected to lack

Shh-dependent cell types in the neural tube. *Ift122*^{sopb} is a null allele of the gene encoding IFT122 [32], which is a core component of the IFT-A complex [37]. Contrary to our expectation, embryos homozygous for both *Dync2h1*^{lln} and the null allele *Ift122*^{sopb} showed ectopic activity of the Shh pathway in the neural tube, similar to the phenotype of *Ift122*$^{sopb/sopb}$ single mutants (Fig. 4a, Supplementary Fig. 7). The motor neuron marker HB9 was expressed in a dorsally expanded domain in the double mutants, as in *Ift122*$^{sopb/sopb}$ single mutants (Fig. 4a). Floor plate and V3 progenitors, which were absent in *Dync2h1*$^{lln/lln}$ embryos (Fig. 1b), were specified in the double mutants, although these domains did not show the dorsal expansion seen in *Ift122*$^{sopb/sopb}$ single mutants (Fig. 4a). Thus, in the context of this IFT-A mutant, the Shh pathway can be ectopically activated to high levels even in the absence of the canonical retrograde motor.

Just as the neural patterning of the double mutants resembled that of *Ift122*$^{sopb/sopb}$, the *Dync2h1*$^{lln/lln}$ *Ift122*$^{sopb/sopb}$ double mutant cilia were similar to those of the *Ift122*$^{sopb/sopb}$ single mutants (Fig. 4b, Supplementary Table 1). IFT88 was enriched at cilia tips (Fig. 4c), as in *Ift122*$^{sopb/sopb}$ single mutants, and not accumulated along the cilium as seen in *Dync2h1*$^{lln/lln}$ cilia (Fig. 1c). Smo was localized to cilia only in the presence of Shh (Fig. 4d), and Gli2 was limited to the tips of *Dync2h1*$^{lln/lln}$ *Ift122*$^{sopb/sopb}$ double mutant cilia (Fig. 4e). Thus removal of this IFT-A protein prevented the accumulation of proteins within the cilium caused by loss of Dync2h1, suggesting that Ift122 has a role in anterograde, as well as retrograde trafficking.

Dync2h1 protein was enriched at the base of the cilium and in puncta along in the axoneme of wild-type MEFs (Fig. 4f), as in *Chlamydomonas* [25,26]. In contrast, Dync2h1 protein accumulated near the base of *Ift122*^{sopb} mutant cilia with little or no staining along the distal axoneme (Fig. 4f). This suggests that the defect in retrograde trafficking in *Ift122*^{sopb} mutants might be due to a failure of the retrograde motor to enter the cilium normally. The loss of Dync2h1 from the *Ift122*$^{sopb/sopb}$ cilium could account for the similarity between the *Dync2h1*$^{lln/lln}$ *Ift122*$^{sopb/sopb}$ double and *Ift122*$^{sopb/sopb}$ single mutant phenotypes.

Lowered dosage of Ift122 suppresses the *Dync2h1* phenotype and restores Shh responsiveness

As with the IFT-B complex genes, removal of one copy of *Ift122* partially rescued the phenotype of *Dync2h1* homozygotes. All ventral neural cell types, including floor plate, V3 progenitors and motor neurons, were specified in the caudal neural tube in the *Dync2h1*$^{lln/lln}$ *Ift122*^{sopb}/+ embryos (Fig. 5).

Two alternative models could explain the suppression of the *Dync2h1* phenotype by decreased dosage of *Ift122*. In the first model, Dync2h1 and IFT122 have opposing phenotypes because they have opposing effects on the activity of core Hh pathway components and the suppression reflects a balance of these effects. Both *Ift122* and *Dync2h1* act downstream of Shh, Patched1 and Smoothened [32](Supplementary Fig. 1a), so this model predicts that Ift122 and Dync2h1 have opposing effects on the activity of pathway proteins downstream of Smo; in this case, the suppression of the *Dync2h1* phenotype would be independent of the presence of ligand. Alternatively, the suppression could indicate that changing the balance of IFT proteins restored sensitivity to Shh ligand. We therefore tested

whether activation of the pathway in *Dync2h1*$^{lln/lln}$ *Ift122*^{sopb}/+ embryos depended on Shh. The external morphology of *Dync2h1*$^{lln/lln}$ *Ift122*^{sopb}/+ *Shh*$^{-/-}$ mutants appeared to be intermediate between *Dync2h1*$^{lln/lln}$ *Ift122*^{sopb}/+ and *Shh*$^{-/-}$ embryos (Fig. 5). In the neural tube, markers of the FP and V3 progenitors, which were expressed in *Dync2h1*$^{lln/lln}$ *Ift122*^{sopb}/+ embryos, were not expressed in *Dync2h1*$^{lln/lln}$ *Ift122*^{sopb}/+ *Shh*$^{-/-}$ compound mutants. Thus the specification of ventral neural cell types in *Dync2h1*$^{lln/lln}$ *Ift122*^{sopb}/+ embryos depended on the presence of Shh (Fig. 5, Supplementary Fig. 8). This suggests that the suppression of the *Dync2h1* phenotype was not due to a direct effect on the activity of core components of the Shh pathway and was instead due to a change in the balance of IFT trafficking.

Consistent with the model that reduced IFT122 suppressed the *Dync2h1* phenotype because of the altered balance of IFT, cilia phenotypes were also strongly rescued by lowering the dosage of *Ift122: Dync2h1*$^{lln/lln}$ *Ift122*^{sopb}/+ compound mutant neural cilia were less wide than *Dync2h1*$^{lln/lln}$ cilia (Fig. 6a, Supplementary Table 1). Trafficking of IFT88 (Fig. 6b, Supplementary Fig. 9a, Supplementary Table 2) and the Hh components Smo (Fig. 6c, Supplementary Fig. 9b) and Gli2 (Fig. 6d, Supplementary Fig. 9c, Supplementary Table 3) was also rescued in the compound mutant MEFs. Smo was found in cilia of *Dync2h1*$^{lln/lln}$ *Ift122*^{sopb}/+ MEFs only after cells were exposed to Shh (Fig. 6c, Supplementary Fig. 9b) and Gli2 was enriched in cilia tips only after stimulation with Shh (Fig. 6d, Supplementary Fig. 9c, Supplementary Table 3). Therefore partial loss of *Ift122* rescued the *Dync2h1* trafficking defect, restoring normal cilia morphology and normal ciliary localization of Hh pathway proteins (Fig. 6e). The restored trafficking of Gli2 and Smo in MEFs also paralleled the ligand-dependent specification of ventral neural cell types in *Dync2h1*$^{lln/lln}$ *Ift122*^{sopb}/+ embryos (Fig. 5). In addition, *Ift122*^{sopb}/+ rescues the ectopic localization of Smo in neural cilia seen in *Dync2h1*$^{lln/lln}$ embryos: Smo is present in cilia only in the ventral neural tube of *Dync2h1*$^{lln/lln}$ *Ift122*^{sopb}/+ embryos (Supplementary Fig. 10). Thus normal Shh-dependent protein trafficking in cilia and neural patterning can take place in the absence of Dync2h1, if the dosage of *Ift122* is reduced.

Discussion

Our studies suggest that the roles of IFT proteins in Shh signaling depend, in large part, on their importance in cilia structure. While both IFT-dynein and IFT-B complex proteins are required for Shh signaling, we find that reduction of IFT-B complex protein levels can suppress the defects in the Shh pathway defects and cilia morphology caused by loss IFT-dynein. The most striking rescue of the *Dync2h1*$^{lln/lln}$ phenotype was seen by lowering the amount of IFT172 to ∼60% of wild-type levels. Neural patterning in the caudal neural tube is indistinguishable from wild type in *Dync2h1*$^{lln/lln}$ *Ift172*^{avc1}/+ embryos. In contrast to the midgestation lethality of *Dync2h1*$^{lln/lln}$ embryos, the compound mutants survive to at least E16.5 when most of the phenotypes associated with defects in Hh signaling, such as polydactyly, are mitigated.

The rescue of Shh signaling in the compound mutants correlates with the rescue of cilia structure. *Dync2h1* mutant cilia that accumulate IFT proteins, Smo, Ptch1 and Gli2 to high levels, but downstream Hh targets are not activated in the *Dync2h1* mutant neural tube. In

contrast, *Dync2h1*$^{lln/lln}$ *Ift172*^{avc1}/+ cilia have normal morphology and do not accumulate either IFT or Hh pathway proteins, and Hh target gene expression appears to be normal. We therefore conclude that the defect in Shh signal transduction in *Dync2h1*$^{lln/lln}$ mutants is caused by a block of retrograde trafficking that disrupts the architecture of the cilium due to the accumulation of IFT-B and other ciliary proteins, and that IFT-dynein does not play a direct role in transporting Gli proteins from the tip to the base of the cilium.

Because double mutants that lack both IFT-dynein and the IFT-A protein IFT122 have cilia that resemble those of the *Ift122* single mutant, we suggest that *Dync2h1* and *Ift122* mutants share a common defect in retrograde trafficking, and that IFT122 has additional roles in the cilium. Like the IFT-B genes, reduced dosage of *Ift122* suppresses the *Dync2h1* phenotype, which suggests the IFT-A complex has a role in anterograde ciliary trafficking. Similarly, recent findings in *Chlamydomonas* show that while partial loss of IFT-A function causes preferential defects in retrograde trafficking, complete loss of IFT-A leads to loss of flagella [35,38]. We suggest the gain of Hh phenotype seen in IFT-A mutants occurs either because IFT-A is required to load unidentified Hh pathway antagonists into the cilium [32,37] or because the structure of the cilium is altered in IFT-A mutants in a way that disrupts the normal interactions between Hh pathway proteins.

Our findings show that lowered levels of two IFT-B complex genes and one IFT-A complex gene strongly suppress the *Dync2h1* phenotype in the mouse. Although previous studies have shown that mutations in cilia-associated genes can have additive effects [1-5], this is the first demonstration that mutations in one set of cilia genes can suppress the phenotype of mutations that affect another aspect of ciliary trafficking. It is striking that although mutations in human *IFT122* cause cranioectodermal dyplasia [39], a ciliopathy that partially overlap with JATD, our data predict that heterozygosity for human *IFT122* would partially correct the defects seen in JATD caused by mutations in *DYNC2H1*. As hundreds of genes are required for the formation of primary cilia, it is possible that the variable expressivity of human *DYNC2H1* mutations could be due to heterozygosity for mutations in other cilia genes. It will be important to consider this type of dosage-sensitive genetic interaction when analyzing whole exome sequence data to identify genes responsible for ciliopathies and other complex genetic disorders [40].

Methods

Antibodies

Smo and Ptch1 antibodies were raised in rabbits (Pocono Rabbit Farm and Laboratory Inc.) using antigens and procedures described previously [17]; both antibodies were used at a dilution of 1:500. Monoclonal antibodies against Nkx2.2 (74.5A5), HB9/MNR2 (81.5C10) and Pax6 (PAX6) were used at 1:10 and obtained from the Developmental Studies Hybridoma Bank. In all experiments, ciliary microtubules were marked by expression of acetylated α-tubulin (mouse, 1:5000, Sigma Aldrich). Other antibodies used were: FoxA2 (rabbit, 1:200, Abcam), Olig2 (rabbit, 1:200, Millipore), γ tubulin (mouse, 1:5000, Sigma Aldrich), IFT88 (rabbit, 1:500, Proteintech). The Gli2 antibody was described previously [41] (guinea pig, 1:500); antibodies that recognize Dync2h1 [42] (rabbit, 1:200) were a gift from R. Vallee (Columbia University).

Mouse Mutations and Strains

Genotyping for the *Dync2h1* alleles *ling-ling (lln)*, *tian-tian* (*ttn*) and *mei-mei (mmi)* as well as the genetrap line *Dync2h1*$^{Gt(RRM278)Byg}$ were described previously [15,23,43]. All *Dync2h1* alleles were maintained in a C3H background, with the exception of *mmi*, which was analyzed in the FVB background. At least three embryos for each genotype described were examined for both neural patterning and cilia structure.

Ift172^{avc1} is an A to G transition in the splice donor site upstream of exon 24 [29]; this change creates a *DraIII* restriction fragment length polymorphism when assayed in genomic DNA using the allele-specific primer wmp-G1. The *Ift122*^{sopb} mutation is a C to T transition in the start codon and destroys a *BtgZI* restriction site assayed using allele-specific primer sopb-G1 to genotype genomic DNA. *Ift172*^{wim} genotyping has been described previously [16,31]. The *Ift88*^{null} allele used in Supplementary Fig. 6 was generated by crossing the conditional *Ift88* allele [44] to the CAG-Cre line [45]. Genotyping of the *Shh*^{tm1Chg}, *Ptch1*^{tm1Mps}, *Gli3*$^{Xt\text{-}J}$ and *Gli2*^{tm1Alj} mutant alleles was carried out as described [46-49].

Primary MEF cell culture

MEFs were isolated from E10.5 embryos as described [23]. Cells were maintained in High Glucose DMEM, 0.05 mg/ml Penicillin, 0.05 mg/ml Streptomycin, 2 mM L-Glutamine, and 10% Fetal Bovine Serum (FBS). Cells were shifted from 10% to 0.5% FBS 24-48h after plating to induce ciliogenesis. Shh stimulation was initiated 24h post starvation using Shh-conditioned medium (used at 1:5 dilution in low-serum medium) for an additional 24h as described [23].

Cells were fixed in 4% Paraformaldehyde (PFA) in Phosphate Buffered Saline (PBS) for 15 minutes and washed extensively in PBS + 0.1% Triton X-100 (PBT). Fixed cells were placed in blocking solution (PBT + 1% v/v FBS) for 10 minutes. Cells were then incubated with primary antibodies diluted in blocking solution overnight at 4°C. The next day, cells were washed three times in PBT and incubated with Alexa-coupled secondary antibodies and DAPI in blocking solution for 1 hour at room temperature. After washing three times in PBT, cells were mounted in Vectashield for microscopy. For Dync2h1 staining, cells were fixed in cold methanol at -20°C for 5 minutes after fixation in 4% PFA. Processing for immunofluorescence proceeded as described above.

Light microscopy

Cilia images were obtained using a DeltaVision image restoration microscope (Applied Precision/Olympus) equipped with CoolSnap QE cooled CCD camera (Photometrics). An Olympus 100×/1.40 NA, UPLS Apo oil immersion objective was used. Z-stacks were taken at 0.20-μm intervals. Images were deconvolved using the SoftWoRx software (Applied Precision/DeltaVision) and corrected for chromatic aberrations.

Confocal microscopy was performed using an upright Leica TCS SP2 AOBS laser scanning microscope. Images were taken with a 63× water objective and 1× zoom. Extended views of the confocal datasets were processed using the Volocity software package (Improvision).

Scanning Electron Microscopy

E10.5 embryos were dissected in PBS at RT and immediately fixed in 2.5% glutaraldehyde and 2% PFA in 0.1M Sodium Cacodylate Buffer, pH 7.4 (Electron Microscopy Sciences) for at least 1 hr at RT. Embryos were stored in fixative for an additional 24 hr at 4°C before processing as described previously [16]. Scanning electron micrograph images were taken on a Zeiss SUPRA 25 FESEM.

Cilia measurements

Cilia lengths and widths were measured from a series of representative SEM images of primary cilia located 15-60μm from the ventral midline acquired at 30,000× and 50,000× magnifications. All measurements were processed using ImageJ Software (NIH Image). Length was measured from the tip of cilia to the base. Width was measured from one side of cilia to the other at its widest point. At least three embryos per genotype were analyzed for measurement and at least 30 images were taken for each embryo; total number of cilia counted is indicated in the tables. Non-deconvolved confocal images were used for quantitative analysis of IFT88 and Gli2 immunofluorescence within cilia. Using Metamorph software (Molecular Devices, Downington, PA), a region of interest (ROI) was created using the acetylated α-tubulin channel and transposed to the IFT88 or Gli2 channel and integrated density was measured and reported as arbitrary units (a.u.).

Supplementary Material

Refer to Web version on PubMed Central for supplementary material.

Acknowledgments

We thank Richard Vallee (Columbia University College of Physicians and Surgeons, New York) for the Dync2h1 antibody, Rajat Rohatgi and Matthew Scott (Stanford University, Palo Alto, CA) for expression constructs used to generate antibodies against Smo and Ptch1, and Scott Weatherbee for help in antibody production. We thank Brad Yoder (University of Alabama at Birmingham) for the mouse *Ift88* conditional allele and Alexandra Joyner (MSKCC, New York) for *Gli2* and *Gli3*$^{Xt J}$ mice. We acknowledge Nina Lampen (MSKCC Electron Microscopy Facility) for technical support with scanning electron microscopy; Zsolt Lazar, Yevgeniy Romin and Sho Fujisawa (MSKCC Molecular Cytology Core) for assistance with confocal microscopy and Metamorph analysis, and Shawn Galdeen (Rockefeller University Bio-Imaging Resource Center) for assistance with Deltavision microscopy. We are grateful to members of the Anderson lab and Timothy Bestor (Columbia University Medical Center) for helpful discussions and critical reading of the manuscript. Monoclonal antibodies were obtained from the Developmental Studies Hybridoma Bank, which was developed under the auspices of the National Institute of Child Health and Human Development and is maintained by the Department of Biological Sciences, University of Iowa. This work was supported by the National Institutes of Health R01 NS044385 to KVA.

References

1. Badano JL, et al. Dissection of epistasis in oligogenic Bardet-Biedl syndrome. Nature. 2006; 439:326–30. [PubMed: 16327777]
2. Hoefele J, et al. Evidence of oligogenic inheritance in nephronophthisis. J Am Soc Nephrol. 2007; 18:2789–95. [PubMed: 17855640]
3. Katsanis N, et al. Triallelic inheritance in Bardet-Biedl syndrome, a Mendelian recessive disorder. Science. 2001; 293:2256–9. [PubMed: 11567139]
4. Khanna H, et al. A common allele in RPGRIP1L is a modifier of retinal degeneration in ciliopathies. Nat Genet. 2009; 41:739–45. [PubMed: 19430481]

5. Leitch CC, et al. Hypomorphic mutations in syndromic encephalocele genes are associated with Bardet-Biedl syndrome. Nat Genet. 2008; 40:443–8. [PubMed: 18327255]
6. Baker K, Beales PL. Making sense of cilia in disease: the human ciliopathies. Am J Med Genet C Semin Med Genet. 2009; 151C:281–95. [PubMed: 19876933]
7. Gherman A, Davis EE, Katsanis N. The ciliary proteome database: an integrated community resource for the genetic and functional dissection of cilia. Nat Genet. 2006; 38:961–2. [PubMed: 16940995]
8. Inglis PN, Boroevich KA, Leroux MR. Piecing together a ciliome. Trends Genet. 2006; 22:491–500. [PubMed: 16860433]
9. Dagoneau N, et al. DYNC2H1 mutations cause asphyxiating thoracic dystrophy and short rib-polydactyly syndrome, type III. Am J Hum Genet. 2009; 84:706–11. [PubMed: 19442771]
10. Merrill AE, et al. Ciliary abnormalities due to defects in the retrograde transport protein DYNC2H1 in short-rib polydactyly syndrome. Am J Hum Genet. 2009; 84:542–9. [PubMed: 19361615]
11. Pedersen LB, Rosenbaum JL. Intraflagellar transport (IFT) role in ciliary assembly, resorption and signalling. Curr Top Dev Biol. 2008; 85:23–61. [PubMed: 19147001]
12. Ho NC, Francomano CA, van Allen M. Jeune asphyxiating thoracic dystrophy and short-rib polydactyly type III (Verma-Naumoff) are variants of the same disorder. Am J Med Genet. 2000; 90:310–4. [PubMed: 10710229]
13. Goetz SC, Anderson KV. The primary cilium: a signalling centre during vertebrate development. Nat Rev Genet. 2010; 11:331–44. [PubMed: 20395968]
14. Weatherbee SD, Niswander LA, Anderson KV. A mouse model for Meckel syndrome reveals Mks1 is required for ciliogenesis and Hedgehog signaling. Hum Mol Genet. 2009; 18:4565–75. [PubMed: 19776033]
15. Huangfu D, Anderson KV. Cilia and Hedgehog responsiveness in the mouse. Proc Natl Acad Sci U S A. 2005; 102:11325–30. [PubMed: 16061793]
16. Huangfu D, et al. Hedgehog signalling in the mouse requires intraflagellar transport proteins. Nature. 2003; 426:83–7. [PubMed: 14603322]
17. Rohatgi R, Milenkovic L, Scott MP. Patched1 regulates hedgehog signaling at the primary cilium. Science. 2007; 317:372–6. [PubMed: 17641202]
18. Corbit KC, et al. Vertebrate Smoothened functions at the primary cilium. Nature. 2005; 437:1018–21. [PubMed: 16136078]
19. Haycraft CJ, et al. Gli2 and Gli3 localize to cilia and require the intraflagellar transport protein polaris for processing and function. PLoS Genet. 2005; 1:e53. [PubMed: 16254602]
20. Chen MH, et al. Cilium-independent regulation of Gli protein function by Sufu in Hedgehog signaling is evolutionarily conserved. Genes Dev. 2009; 23:1910–28. [PubMed: 19684112]
21. Wen X, et al. Kinetics of Hedgehog-dependent full-length Gli3 accumulation in primary cilia and subsequent degradation. Mol Cell Biol. 2010
22. May SR, et al. Loss of the retrograde motor for IFT disrupts localization of Smo to cilia and prevents the expression of both activator and repressor functions of Gli. Dev Biol. 2005; 287:378–89. [PubMed: 16229832]
23. Ocbina PJ, Anderson KV. Intraflagellar transport, cilia, and mammalian Hedgehog signaling: analysis in mouse embryonic fibroblasts. Dev Dyn. 2008; 237:2030–8. [PubMed: 18488998]
24. Tran PV, et al. THM1 negatively modulates mouse sonic hedgehog signal transduction and affects retrograde intraflagellar transport in cilia. Nat Genet. 2008; 40:403–10. [PubMed: 18327258]
25. Pazour GJ, Dickert BL, Witman GB. The DHC1b (DHC2) isoform of cytoplasmic dynein is required for flagellar assembly. J Cell Biol. 1999; 144:473–81. [PubMed: 9971742]
26. Perrone CA, et al. A novel dynein light intermediate chain colocalizes with the retrograde motor for intraflagellar transport at sites of axoneme assembly in chlamydomonas and Mammalian cells. Mol Biol Cell. 2003; 14:2041–56. [PubMed: 12802074]
27. Porter ME, Bower R, Knott JA, Byrd P, Dentler W. Cytoplasmic dynein heavy chain 1b is required for flagellar assembly in Chlamydomonas. Mol Biol Cell. 1999; 10:693–712. [PubMed: 10069812]

28. Kim J, Kato M, Beachy PA. Gli2 trafficking links Hedgehog-dependent activation of Smoothened in the primary cilium to transcriptional activation in the nucleus. Proc Natl Acad Sci U S A. 2009
29. Friedland-Little JM, et al. A novel allele of Intraflagellar Transport Protein 172 implicates VACTERL with hydrocephalus as a ciliopathy in mice. submitted. 2010
30. Kamp A, et al. Genome-wide Identification of Mouse Congenital Heart Disease Loci. Hum Mol Genet. 2010
31. Eggenschwiler JT, Espinoza E, Anderson KV. Rab23 is an essential negative regulator of the mouse Sonic hedgehog signalling pathway. Nature. 2001; 412:194–8. [PubMed: 11449277]
32. Qin J, Lin Y, Norman RX, Ko HW, Eggenschwiler JT. Intraflagellar transport protein 122 antagonizes Sonic Hedgehog signaling and controls ciliary localization of pathway components. Proc Natl Acad Sci U S A. 2011; 108:1456–61. [PubMed: 21209331]
33. Liu A, Wang B, Niswander LA. Mouse intraflagellar transport proteins regulate both the activator and repressor functions of Gli transcription factors. Development. 2005; 132:3103–11. [PubMed: 15930098]
34. Iomini C, Babaev-Khaimov V, Sassaroli M, Piperno G. Protein particles in Chlamydomonas flagella undergo a transport cycle consisting of four phases. J Cell Biol. 2001; 153:13–24. [PubMed: 11285270]
35. Iomini C, Li L, Esparza JM, Dutcher SK. Retrograde intraflagellar transport mutants identify complex A proteins with multiple genetic interactions in Chlamydomonas reinhardtii. Genetics. 2009; 183:885–96. [PubMed: 19720863]
36. Cortellino S, et al. Defective ciliogenesis, embryonic lethality and severe impairment of the Sonic Hedgehog pathway caused by inactivation of the mouse complex A intraflagellar transport gene Ift122/Wdr10, partially overlapping with the DNA repair gene Med1/Mbd4. Dev Biol. 2009; 325:225–37. [PubMed: 19000668]
37. Mukhopadhyay S, et al. TULP3 bridges the IFT-A complex and membrane phosphoinositides to promote trafficking of G protein-coupled receptors into primary cilia. Genes Dev. 2010; 24:2180–93. [PubMed: 20889716]
38. Piperno G, et al. Distinct mutants of retrograde intraflagellar transport (IFT) share similar morphological and molecular defects. J Cell Biol. 1998; 143:1591–601. [PubMed: 9852153]
39. Walczak-Sztulpa J, et al. Cranioectodermal Dysplasia, Sensenbrenner syndrome, is a ciliopathy caused by mutations in the IFT122 gene. Am J Hum Genet. 2010; 86:949–56. [PubMed: 20493458]
40. Zaghloul NA, Katsanis N. Functional modules, mutational load and human genetic disease. Trends Genet. 2010; 26:168–76. [PubMed: 20226561]
41. Cho A, Ko HW, Eggenschwiler JT. FKBP8 cell-autonomously controls neural tube patterning through a Gli2- and Kif3a-dependent mechanism. Dev Biol. 2008; 321:27–39. [PubMed: 18590716]
42. Mikami A, et al. Molecular structure of cytoplasmic dynein 2 and its distribution in neuronal and ciliated cells. J Cell Sci. 2002; 115:4801–8. [PubMed: 12432068]
43. Liem KF Jr, He M, Ocbina PJ, Anderson KV. Mouse Kif7/Costal2 is a cilia-associated protein that regulates Sonic hedgehog signaling. Proc Natl Acad Sci U S A. 2009; 106:13377–82. [PubMed: 19666503]
44. Haycraft CJ, et al. Intraflagellar transport is essential for endochondral bone formation. Development. 2007; 134:307–16. [PubMed: 17166921]
45. Sakai K, Miyazaki J. A transgenic mouse line that retains Cre recombinase activity in mature oocytes irrespective of the cre transgene transmission. Biochem Biophys Res Commun. 1997; 237:318–24. [PubMed: 9268708]
46. Chiang C, et al. Cyclopia and defective axial patterning in mice lacking Sonic hedgehog gene function. Nature. 1996; 383:407–13. [PubMed: 8837770]
47. Mo R, et al. Specific and redundant functions of Gli2 and Gli3 zinc finger genes in skeletal patterning and development. Development. 1997; 124:113–23. [PubMed: 9006072]
48. Goodrich LV, Milenkovic L, Higgins KM, Scott MP. Altered neural cell fates and medulloblastoma in mouse patched mutants. Science. 1997; 277:1109–13. [PubMed: 9262482]

49. Litingtung Y, Chiang C. Specification of ventral neuron types is mediated by an antagonistic interaction between Shh and Gli3. Nat Neurosci. 2000; 3:979–85. [PubMed: 11017169]

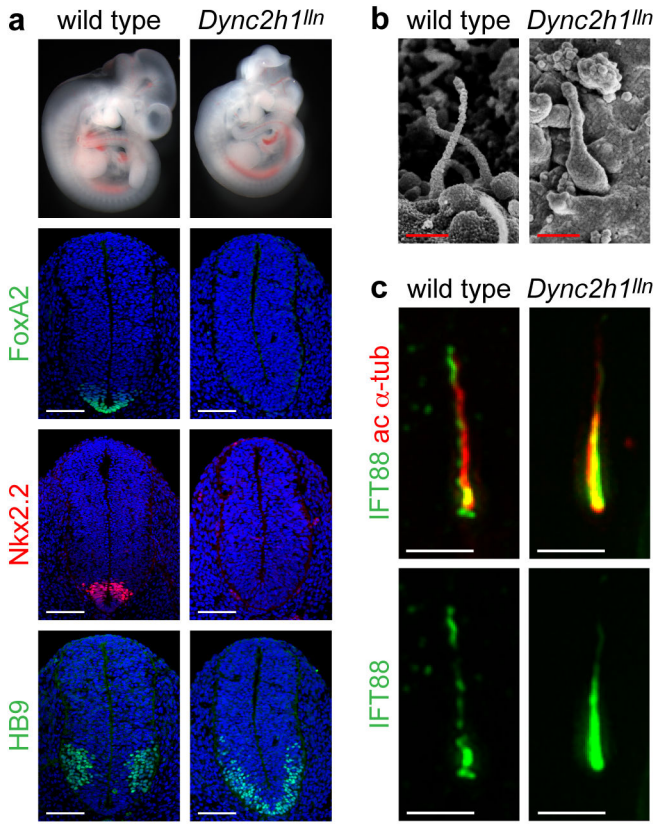

Figure 1. Mutations in *Dync2h1* disrupt Shh-dependent neural patterning and cilia morphology

(**a**), Mutations in *Dync2h1* lead to the absence of Shh-dependent cell types in the E10.5 neural tube. In *Dync2h1*$^{lln/lln}$ mutants, floor plate (FoxA2, green) and V3 progenitor (Nkx2.2, red) domains are not specified, and motor neurons (HB9, green) are present only in the caudal neural tube (shown here); dorsal up. Scale bars represent 100 μm. (**b**), Scanning electron micrographs show that neural tube primary cilia in *Dync2h1*$^{lln/lln}$ mutants are bloated; dimensions are given in Supplementary Table1. Scale bars represent 500 nm. (**c**), IFT88 (green) in cilia of serum-starved wild-type MEFs is enriched at the base and the tip of the cilium, marked with acetylated α-tubulin (red). In *Dync2h1*$^{lln/lln}$ mutant MEFs, the amount of IFT88 in the cilium is increased and is found all along the axoneme. Quantitation is in Supplementary Table 2. Scale bars represent 1 μm (**c**).

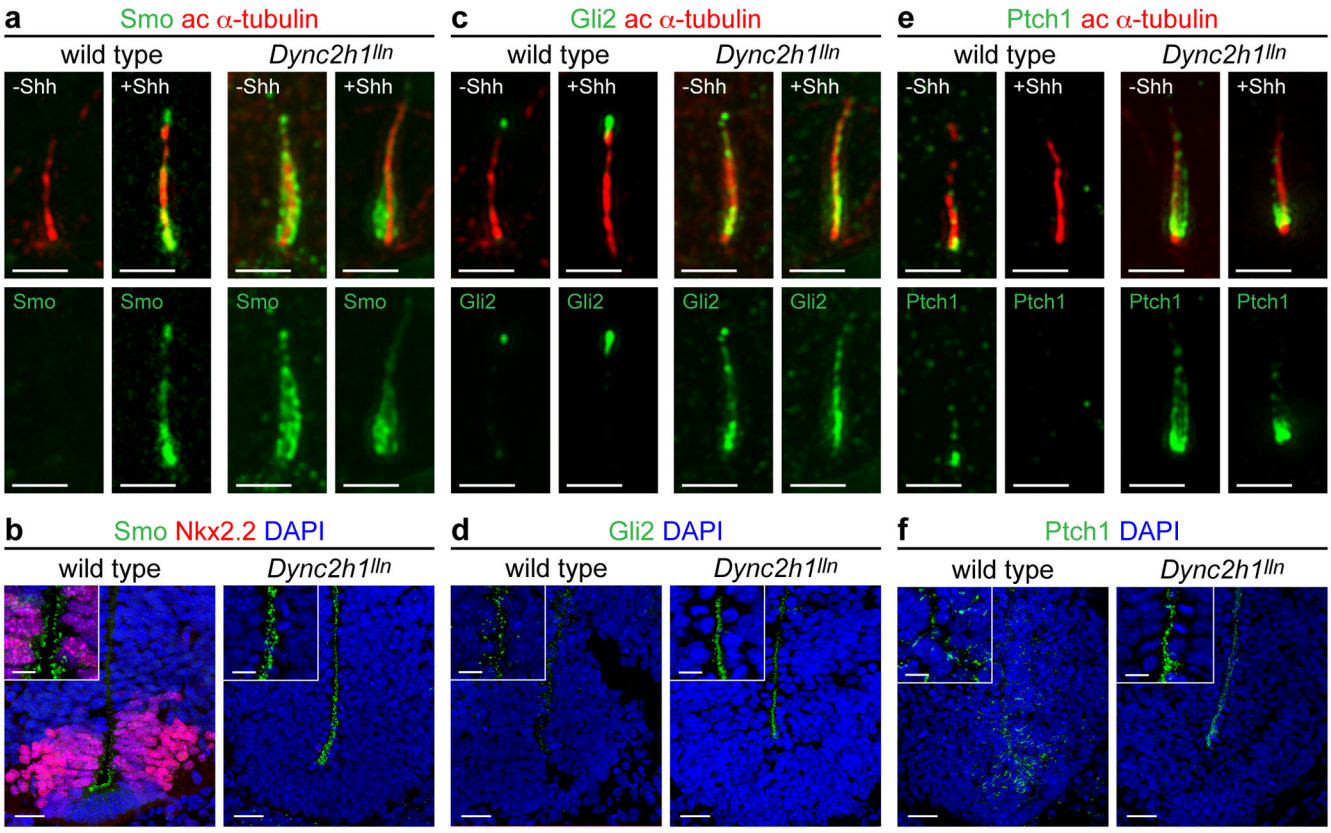

Figure 2. Hh components accumulate in *Dync2h1* mutant cilia

Localization of Smo (**a, b**), Gli2 (**c, d**) and Ptch1 (**e, f**) to the primary cilium in wild-type and *Dync2h1*$^{lln/lln}$ MEFs (**a, c, e**) and E10.5 neural tube (**b, d, f**). (**a**) Smo (green) was enriched in cilia of wild-type MEFs only after exposure to Shh. Smo was enriched in cilia of *Dync2h1*$^{lln/lln}$ mutant cells even in the absence of Shh. (**b**) Smo was enriched in cilia of ventral neural progenitors in wild-type. Smo was strongly enriched in primary cilia of *Dync2h1*$^{lln/lln}$ neural progenitors at all dorsal-ventral levels. (**c**) Gli2 (green) localized to the tips of cilia in wild-type MEFs and accumulated further after Shh treatment. Gli2 levels were elevated along the axoneme of *Dync2h1*$^{lln/lln}$ mutant MEF cilia. (**d**) Gli2 was elevated in the cilia of *Dync2h1*$^{lln/lln}$ neural progenitors. (**e**) Low amounts of endogenous Ptch1 (green) were detected near the base and along the length of primary cilia in wild-type MEFs only in the absence of Shh, whereas Ptch1 was strongly enriched along the axoneme of *Dync2h1*$^{lln/lln}$ cilia in unstimulated cells; strong Ptch1 immunofluorescence remained near the base of the cilium after stimulation with Shh. (**f**) Ptch1 appeared localized to the cytoplasm of wild-type neural progenitors, and was strongly enriched in cilia throughout the neural tube in *Dync2h1*$^{lln/lln}$ mutants. Acetylated α-tubulin (red) marks cilia in (**a, c, e**); (**b, d, f**) are ventral views of transverse sections through the ventral half of the neural tube at the level of the forelimb. Scale bars represent 500 nm (**a, c, e**), 25 μm (**b, d, f**) and 10 μm (insets **b, d, f**).

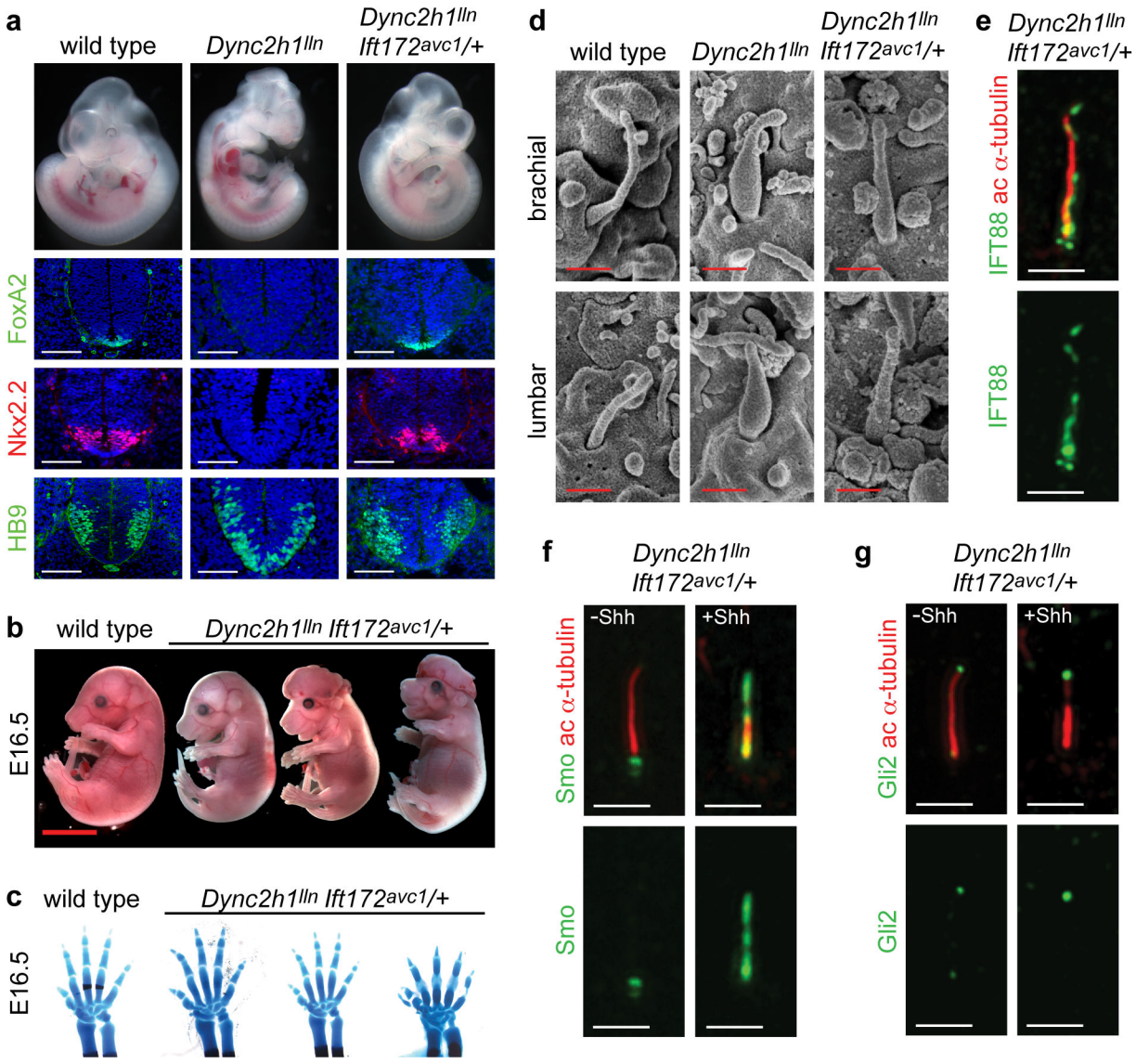

Figure 3. *Ift172* is a dominant suppressor of *Dync2h1*

(**a**), E10.5 embryos and transverse sections through the caudal neural tube of wild-type, *Dync2h1*$^{lln/lln}$ and *Dync2h1*$^{lln/lln}$ *Ift172*^{avc1}/+ embryos. Specification of floor plate (FoxA2, green), V3 progenitors (Nkx2.2, red) and motor neurons (HB9, green) were rescued in *Dync2h1*$^{lln/lln}$ *Ift172*^{avc1}/+ embryos. Scale bars represent 100 μm. (**b**), *Dync2h1*$^{lln/lln}$ *Ift172*^{avc1}/+ mutants survive to at least E16.5 (n=5). Scale bar is 5 mm. (**c**), Right forelimbs and digits of embryos in (**b**) stained with Alcian blue (cartilage) and Alizarin red (bone) staining shows incomplete penetrance of polydactyly in *Dync2h1*$^{lln/lln}$ *Ift172*^{avc1}/+ embryos at E16.5. (**d**), Scanning electron micrographs of cilia from the neural tube at E10.5 showing near-normal morphology of *Dync2h1*$^{lln/lln}$ *Ift172*^{avc1}/+ mutant cilia (quantitation in Supplementary Table 1). Scale bar is 500 nm. IFT88 (green, **e**) and Smo (green, **f**) and Gli2 (red, **g**) localize normally in primary cilia of MEFs derived from *Dync2h1*$^{lln/lln}$ *Ift172*^{avc1}/+ embryos. Acetylated α-tubulin (red) marks cilia in (**e-g**). Scale bars represent 1 μm in (**e-g**).

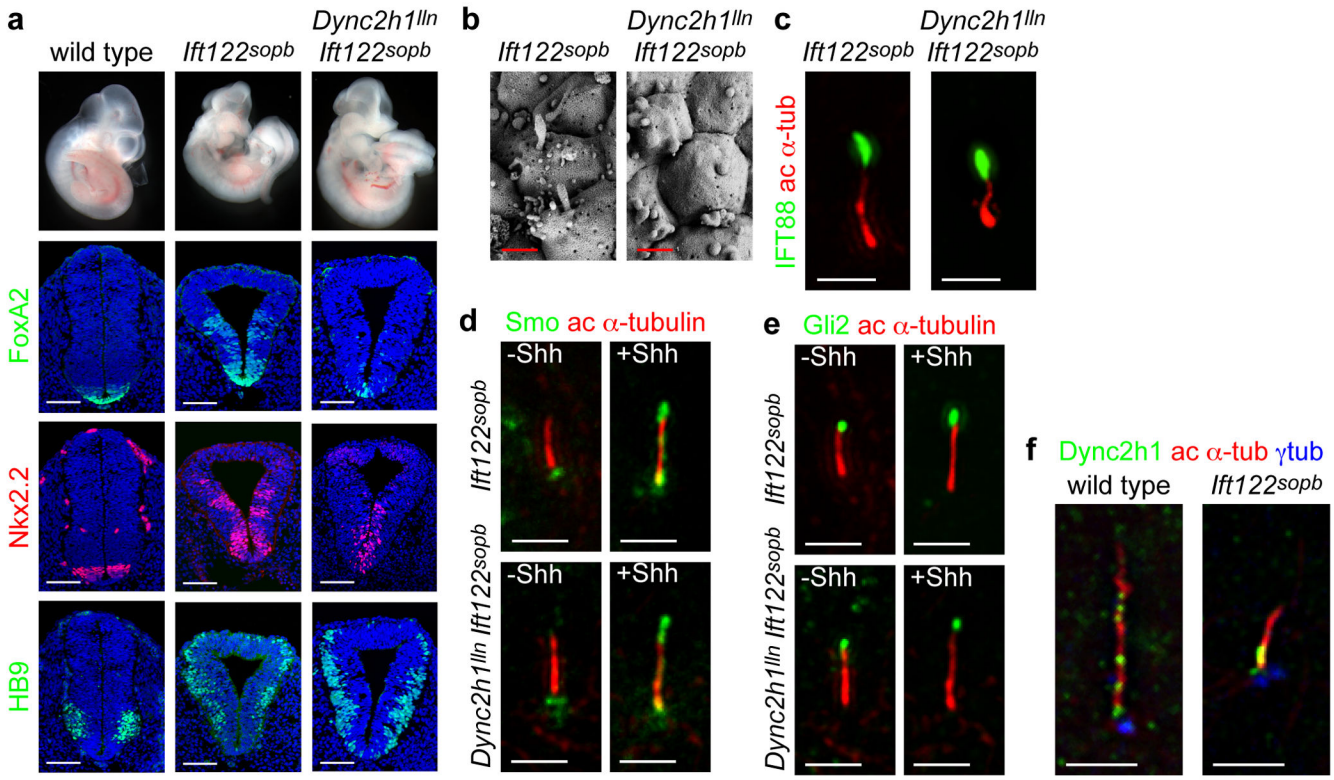

Figure 4. Neural patterning and cilia morphology in *Dync2h1^{lln} Ift122^{sopb}* embryos

(**a**), In contrast to the lack of ventral neural cell types in *Dync2h1$^{lln/lln}$* mutants, both *Ift122$^{sopb/sopb}$* single and *Dync2h1$^{lln/lln}$ Ift122$^{sopb/sopb}$* double mutants specify floor plate (FoxA2, green), V3 progenitors (Nkx2.2, red) and motor neurons (HB9, green) in the lumbar neural tube. Scale bars represent 100 μm. (**b**), Scanning electron micrographs of neural tube cilia from the neural tube of E10.5 *Ift122$^{sopb/sopb}$* and *Dync2h1$^{lln/lln}$ Ift122$^{sopb/sopb}$* embryos. The distal ends of *Ift122$^{sopb/sopb}$* mutant cilia appeared swollen. *Dync2h1$^{lln/lln}$ Ift122$^{sopb/sopb}$* mutant cilia were similar in diameter to *Ift122$^{sopb/sopb}$* but were shorter than either *Dync2h1$^{lln/lln}$* or *Ift122$^{sopb/sopb}$* single mutants (See Supplementary Table 1). Scale bars represent 500 nm. (**c**), IFT88 (green) accumulates specifically at the distal tips of both *Ift122$^{sopb/sopb}$* and *Dync2h1$^{lln/lln}$ Ift122$^{sopb/sopb}$* mutant MEF cilia. Acetylated α-tubulin staining (red) marks primary cilia. Localization of Smo (**d**, green) and Gli2 (**e**, green) in the cilia of *Ift122$^{sopb/sopb}$* and *Dync2h1$^{lln/lln}$ Ift122$^{sopb/sopb}$* mutant MEFs. Acetylated α-tubulin (red) marks cilia. (**f**), Dync2h1 protein is present at the base of the cilium and along the ciliary axoneme in wild-type cells. In *Ift122$^{sopb/sopb}$* mutant cilia, Dync2h1 localization accumulates mainly at the base of the cilium. Orientation for (**b**-**f**) is distal tip up. Scale bars are 1 μm (**d**-**f**).

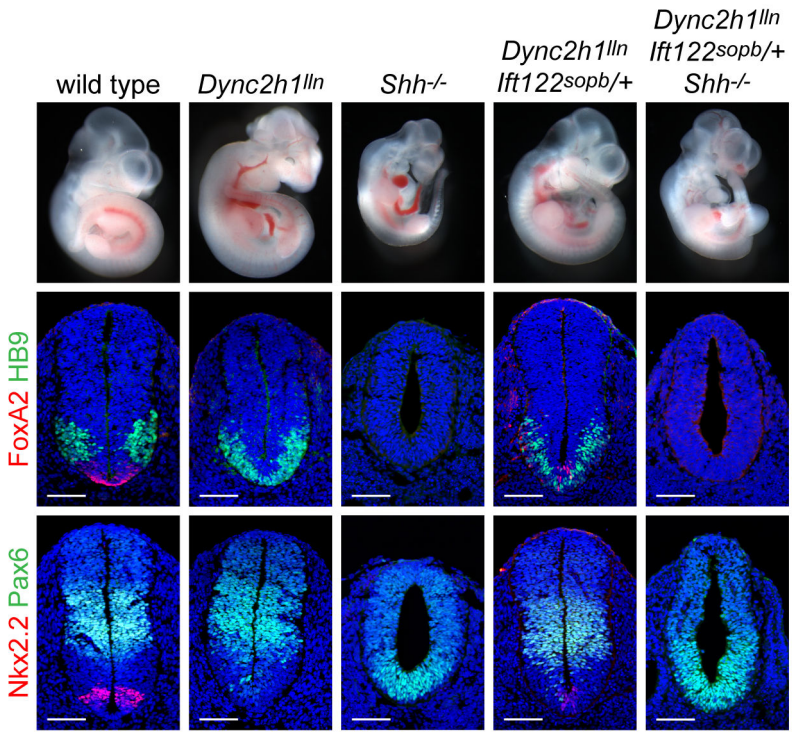

Figure 5. Shh responsiveness in *Dync2h1*$^{lln/lln}$ *Ift122*^{sopb}/+ embryos

Whole embryos and patterning in the lumbar neural tube of E10.5 wild type, *Dync2h1*$^{lln/lln}$, *Shh*$^{-/-}$, *Dync2h1*$^{lln/lln}$ *Ift122*^{sopb}/+ and *Dync2h1*$^{lln/lln}$ *Ift122*^{sopb}/+ *Shh*$^{-/-}$ compound mutants. Specification of floor plate (FoxA2, red, middle panels), V3 progenitors (Nkx2.2, red, bottom panels) and motor neurons (HB9, green, middle panels) were partially rescued in *Dync2h1*$^{lln/lln}$ *Ift122*^{sopb}/+ mutant embryos but all these cell types were absent in *Dync2h1*$^{lln/lln}$ *Ift122*^{sopb}/+ *Shh*$^{-/-}$ embryos. The Pax6 domain (green, bottom panels), which is restricted by low levels of Shh signaling, was ventrally expanded in *Shh*$^{-/-}$ and *Dync2h1*$^{lln/lln}$ *Ift122*^{sopb}/+ *Shh*$^{-/-}$ embryos. Scale bars represent 100 μm.

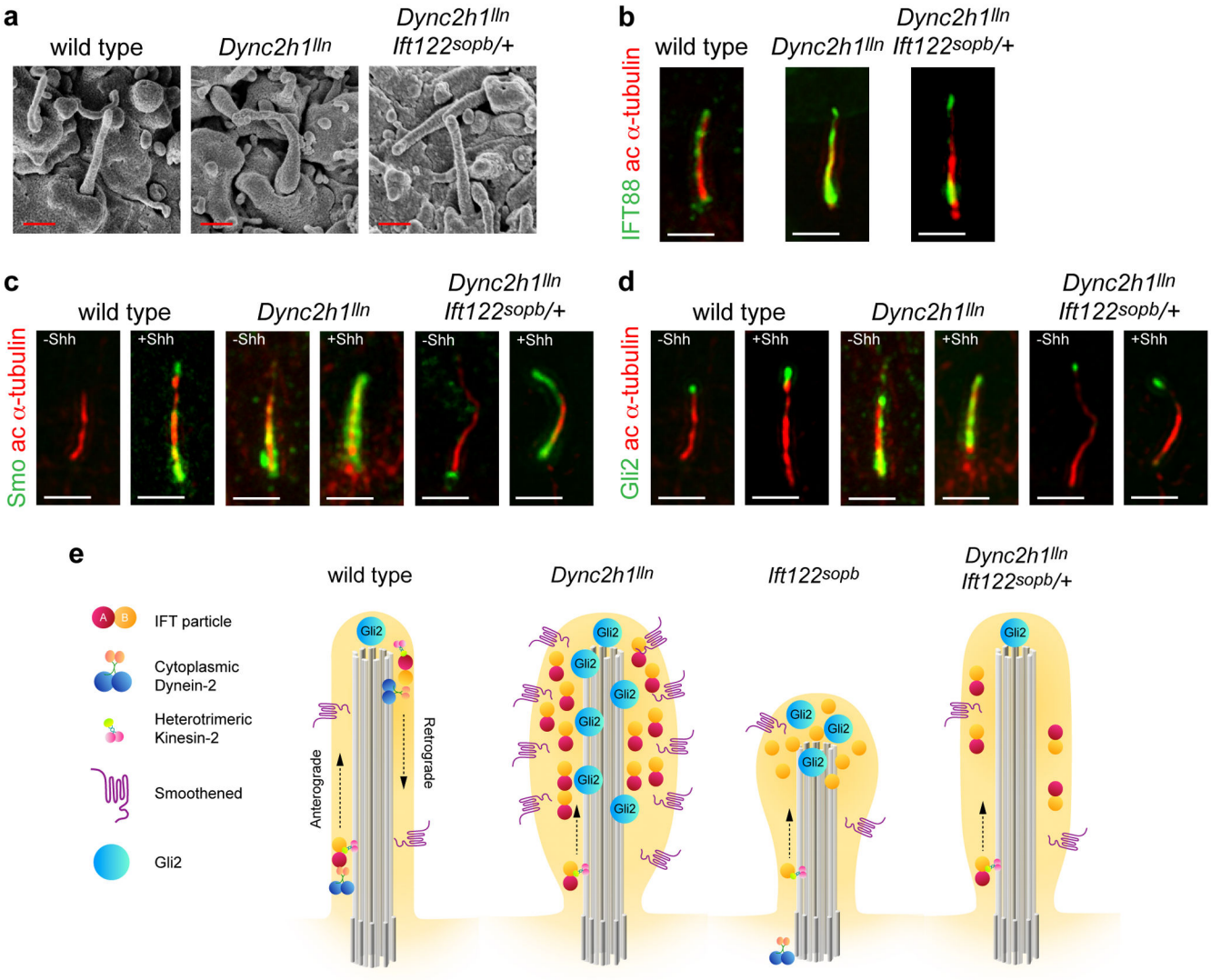

Figure 6. Cilia morphology in *Dync2h1*$^{lln/lln}$ *Ift122*^{sopb}/+ compound mutants

(**a**), SEM analysis of neural tube primary cilia show the more normal length and width of *Dync2h1*$^{lln/lln}$ *Ift122*^{sopb}/+ mutants compared to *Dync2h1*$^{lln/lln}$. Quantitation in Supplementary Table 1. Scale bars are 500 nm. (**b-d**), Localization of IFT88 (**b**, green), Smo (**c**, green) and Gli2 (**d**, green) in cilia (acetylated α-tubulin, red) appear normal in *Dync2h1*$^{lln/lln}$ *Ift122*^{sopb}/+ mutants. Scale bars are 500 nm (**b-d**). (**e**) Model of the trafficking of mammalian IFT and Hh pathway proteins in the primary cilium, shown in the absence of Hh ligand. In wild-type cells, IFT directs the formation of cilia, which accumulate a basal level of Gli2 at cilia tips, while Smo traffics through the cilium at a low basal rate. Loss of retrograde motor in *Dync2h1*$^{lln/lln}$ mutant cilia leads to the accumulation of IFT particles and blocks the movement of both Smo and Gli2 out of the cilium. In *Ift122*$^{sopb/sopb}$ mutants, Dync2h1 protein fails to enter the cilium, leading to the accumulation of IFT-B particles. Loss of IFT122 also results in the accumulation of Gli2 but does not affect Smo trafficking. Decreased anterograde ciliary trafficking in *Dync2h1*$^{lln/lln}$ *Ift122*^{sopb}/+ suppresses the

Dync2h1$^{lln/lln}$ phenotype and permits normal transport of both Smo and Gli2 through the cilium.